Matter

Article

Reconfigurable self-assembly of porous anisotropic colloids in nematic liquid crystals

Graphical abstract

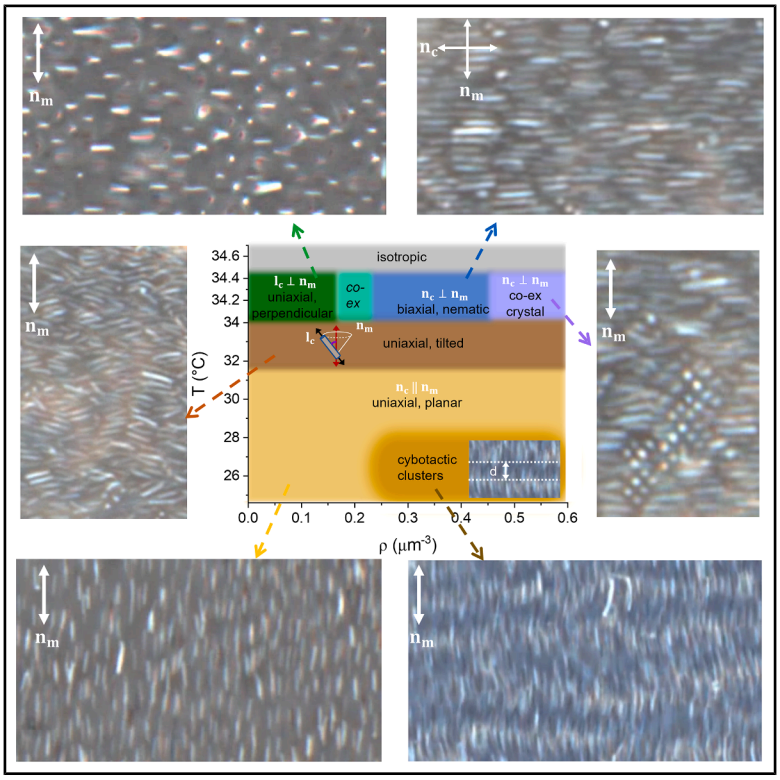

Authors

Souvik Ghosh, Jin-Sheng Wu, Nicholas Golden, Lech Longa, Ivan I. Smalyukh

Correspondence

ivan.smalyukh@colorado.edu

In brief

Mesoporous colloidal microrods dispersed in a uniaxial nematic host fluid exhibit diverse phases of soft matter with thermally reconfigurable point group symmetries, which are of both fundamental and applied interest. The tensorial Landau theory-based model explains our findings and generalizes the possible phase organizations in this hybrid anisotropic molecular-colloidal system. Potential applications range from electro-optics to bio-detection and photonic metamaterial designs.

Highlights

- Mesoporous colloidal rods induce only weak elastic deformations in nematic host fluids
- Numerical modeling captures surface anchoring properties of mesoporous colloidal rods
- Dense dispersions of rods in a nematic host exhibit diverse hybrid soft matter phases
- A tensorial model based on Landau theory rationalizes our experimental observations

3 Understanding
Dependency and conditional studies on material behavior

Ghosh et al., 2026, Matter 9, 102563
March 4, 2026
https://doi.org/10.1016/j.matt.2025.102563

CellPress

Please cite this article in press as: Ghosh et al., Reconfigurable self-assembly of porous anisotropic colloids in nematic liquid crystals, Matter (2025), https://doi.org/10.1016/j.matt.2025.102563

Matter

CellPress

Article

Reconfigurable self-assembly of porous anisotropic colloids in nematic liquid crystals

Souvik Ghosh,[1] Jin-Sheng Wu,[1] Nicholas Golden,[1] Lech Longa,[2,3] and Ivan I. Smalyukh[1,3,4,5,6,*]

[1]Department of Physics, University of Colorado, Boulder, CO 80309, USA

[2]Institute of Theoretical Physics, Department of Statistical Physics and Mark Kac Center for Complex Systems Research, Jagiellonian University, Prof. Stanisława Łojasiewicza 11, 30-348 Kraków, Poland

[3]International Institute for Sustainability with Knotted Chiral Meta Matter (WPI-SKCM^2), Hiroshima University, 1-3-1 Kagamiyama, Higashi, Hiroshima 739-8526, Japan

[4]Department of Electrical, Computer and Energy Engineering and Materials Science and Engineering Program, University of Colorado, Boulder, CO 80309, USA

[5]Renewable and Sustainable Energy Institute, National Renewable Energy Laboratory and University of Colorado, Boulder, CO 80309, USA

[6]Lead contact

*Correspondence: ivan.smalyukh@colorado.edu

https://doi.org/10.1016/j.matt.2025.102563

PROGRESS AND POTENTIAL We have developed a mesostructured soft matter colloidal system with uninhibited 3D orientational fluid order exhibited by co-self-assembled micrometer-sized colloidal and nanometer-sized molecular building blocks, with several unexpected low-symmetry phases. The observed emergent behavior may enable designs of new soft matter composites and high-dimensional-order parameter spaces for using these low-symmetry liquid crystals as model systems for generating topological solitons and singular defects. From an applied perspective, our findings may lead to the design of mesostructured molecular-colloidal composites with pre-engineered physical properties, with potential applications ranging from electro-optics to photonic chips and to biomedical sensing.

SUMMARY

Dispersions of anisotropic nanoparticles in liquid crystalline hosts recently yielded new soft condensed matter states, like the thermally reconfigurable monoclinic and orthorhombic biaxial nematic liquid crystals, with a plethora of unusual phases and phase transformations. Our current study shows that the nanoscale porous nature of colloids with micrometer-range overall dimensions also enables highly reconfigurable orientations and assemblies of the microparticles, allowing for realization of condensed matter states with unusual combinations of low-symmetry nematic or smectic order and fluidity. Much like the anisotropic nanoparticles studied previously, these nanoporous anisotropic colloids exhibit thermally reconfigurable oriented alignment with respect to the far-field director, as well as diverse low-symmetry liquid crystalline phase behaviors. Our findings open doors to fundamental and applied uses of low-symmetry molecular-colloidal orientationally ordered states of matter with uninhibited fluidity, as well as liquid crystals with partial positional ordering, like low-symmetry smectics, which could lead to applications in metamaterial designs, electro-optics, photonics, etc.

INTRODUCTION

Colloidal particles have often been considered as mesoscale mimics of atoms and molecules, providing fundamental insights into the behaviors such as melting of crystals, formation of glasses, or motion of defects within crystals, which for molecular and atomic systems cannot be easily probed experimentally.[1–3] On the other hand, the diversity of naturally occurring atomic and molecular condensed matter states motivated researchers to achieve diverse forms of self-assembly and to use various colloidal structures at the mesoscale in order to control physical behavior of the ensuing self-assembled materials.[4] Recent research efforts have revealed that colloidal- and molecular-scale self-assembly can be synergistically combined to enable forms of ordered condensed matter that cannot be easily achieved in purely molecular or purely colloidal systems, such

Please cite this article in press as: Ghosh et al., Reconfigurable self-assembly of porous anisotropic colloids in nematic liquid crystals, Matter (2025), https://doi.org/10.1016/j.matt.2025.102563

as the monoclinic and orthorhombic nematic liquid crystals (LCs).[5–7] Yet, to date, this behavior could be achieved only for colloidal particles with at least one dimension being nanoscale, e.g., ~10 nm. Micrometer-sized colloidal particles were found inducing topological defects and binding with each other into aggregates of assemblies that could not be dissolved or significantly altered (e.g., in terms of changing symmetry of crystal lattices) by thermal energy or weak stimuli like fields or light.[8–14] At the same time, in isotropic solvents like water, the control of the versatile forms of thermally controlled microcolloidal self-assembly could be more easily accessible.[15] Thus, a major challenge in developing nematic LC microcolloids as forms of pre-designed artificial matter with diverse molecular-colloidal phase behavior relates to the control of the interplay between the orientational elasticity and anisotropic part of surface energy.

Differently from isotropic host media, colloidal interactions and self-assembly in anisotropic liquid crystalline fluid host media strongly depend on the interplay between bulk and surface effects, which is often quantified by the so-called anchoring extrapolation length describing the competition between the bulk orientational elasticity and anisotropic component of surface energy, dubbed "anchoring."[4] Colloidal particles larger than this characteristic length scale have been shown to induce topological defects and form assemblies with interparticle binding and orientations that cannot be significantly altered by thermal energy, thus precluding the possibility of thermal reconfiguration and often the very equilibration from metastable into the lowest-energy states.[4]

In this study, we introduce porous anisotropic nematic colloids that have overall dimensions larger than the extrapolation length but still behave much like their nanoscale colloidal counterparts, which is related to the nanoscale pores within the colloidal objects. The porous nature of colloidal particles allows us to tune the interplay between orientational elasticity and surface anchoring,[16] along with other competing effects, so that the system can form stable colloidal dispersions of particles that freely move one around another, without aggregating. We show that, much like the anisotropic nanoparticles studied previously, these porous anisotropic colloids exhibit thermally reconfigurable oriented alignment with respect to the far-field director of the molecular nematic's host medium, as well as a large variety of low-symmetry liquid crystalline behaviors.

The studied colloidal dispersions form liquid types of assemblies, as well as LCs and crystallites that can be thermally reconfigured. We construct phase diagrams using the temperature-concentration coordinate system, demonstrating emergent phase behavior that can be correlated with the thermal reconfiguration of individual colloids' orientations relative to the far-field director of the molecular host $\mathbf{n}_m$, which describes the average orientation of LC molecules in the uniformly aligned LC medium far from the particles. We characterize the collective behavior of colloids, as well as single-particle-level diffusion within both sparse and various dense colloidal assemblies, revealing emergent soft condensed matter behaviors. To gain insights into the studied phenomena, we model our system's behavior at different levels of the overall soft matter system. First, by considering the host LC medium interacting with a porous particle, we numerically minimize free energy[17–19] to reveal how the porous nature of particles weakens the strength of effective surface anchoring and gives origins to generally oblique local director's easy axis orientation at the porous surfaces, even under conditions when a flat nonporous surface gives tangential or perpendicular anchoring. Then, we analyze equilibrium particle orientations at different effective anchoring conditions controlled by temperature. Finally, we analytically investigate the composite molecular-colloidal system's nematic ordering within the framework of Landau-de Gennes theory,[16,17] which offers insight into the experimentally observed spontaneous symmetry breaking and stabilization of hybrid nematic phases with nonstandard symmetries. We conclude by briefly discussing the potential technological utility of our findings in terms of defining physical behavior via mesoscale control of both molecular and colloidal subsystems.

RESULTS

Experimental design and self-alignment of anisotropic colloids

Rod-shaped cylindrical particles are synthesized using an emulsion-templated wet chemical method.[20,21] Optical microscopy and scanning electron microscopy confirm the production of silica microrods with diameters ranging from 200 to 300 nm and lengths between 2 and 3 μm. Before making dispersions, these microrods undergo a slow etching process by treatment with a 0.5 mM NaOH solution, resulting in the development of an etched porous surface (see Figures 1A and 1B). Subsequently, the microrods are introduced into a nematic LC, pentylcyanobiphenyl (5CB), where the nematic director $\mathbf{n}_m$ represents the average alignment of constituent rod-like molecules.[22] Within these dispersions, the exposed surfaces of the microrods naturally induce tangential (planar) boundary conditions for the nematic director $\mathbf{n}_m$, so that the long axis $\mathbf{l}_c$ of the colloidal particles aligns parallel to it (see Figure 1C). As a result of the interplay between the anisotropic viscoelastic properties of the LC and the geometric shape anisotropy of the oriented particles, the microrods in Figure 1D demonstrate anisotropic translational diffusion ($D_t/D_{t\perp} = 3.37$), where $D_{t\parallel}$ and $D_{t\perp}$ represent the translational diffusion coefficients measured along and perpendicular to the director $\mathbf{n}_m$, respectively.[23,24] Microrods without etching also show similar orientational behavior and translational diffusion anisotropy. However, the probability distribution of angular displacements, tilting away from the energy-minimizing orientation relative to $\mathbf{n}_m$, is lower for regular as-synthesized rods as compared to their etched counterparts (Figure 1E). Another significant difference between the regular and etched rods emerges when they are surface-functionalized with dimethyloctadecyl[3-(trimethoxysilyl)propyl]ammonium chloride (DMOAP), a surfactant that induces homeotropic (locally perpendicular to the surface) boundary conditions for LC molecules. After DMOAP-functionalization, the regular rods exhibit strong perpendicular[25] boundary conditions for $\mathbf{n}_m$, while the etched rods still exhibit tangential surface anchoring even after the DMOAP treatment (refer to Figures S1A and S1B). Furthermore, a stable dispersion of the DMOAP-capped regular rods even at extremely dilute concentrations is difficult to achieve as opposed to the etched rods' case.

Please cite this article in press as: Ghosh et al., Reconfigurable self-assembly of porous anisotropic colloids in nematic liquid crystals, Matter (2025), https://doi.org/10.1016/j.matt.2025.102563

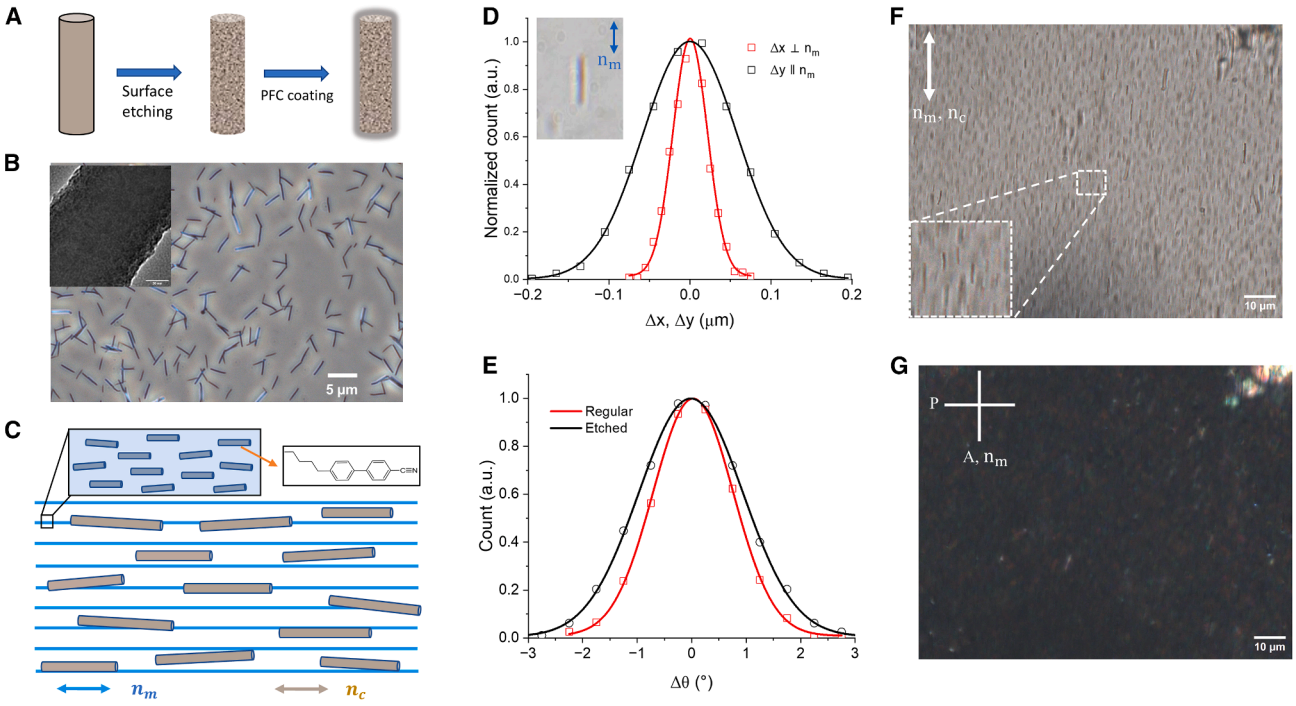

Figure 1. Colloidal microrods in a nematic host of 5CB molecular rods and their characterization

(A) Schematic of the microrods prepared through slow etching, followed by perfluorocarbon (PFC) liquid coating.

(B) Phase-contrast optical microscopy image of the colloidal particles. The inset shows the SEM micrograph highlighting the porous surface of the microrod (scale bar, 30 nm).

(C) Schematic representation of the colloidal particle alignment and colloidal ordering, with the inset showing chemical structure of the rod-like 5CB molecule.

(D) Histograms of the lateral displacements along the *y* axis and perpendicular (*x* axis) to the far-field molecular director $\mathbf{n}_m$.

(E) Histograms of angular displacements for regular as-synthesized and etched microrods freely rotating around $\mathbf{n}_m$ in a planar cell of thickness 50 μm.

(F) Bright-field transmission-mode micrographs of the etched, weak-anchoring microrods, showing their dispersion and alignment along $\mathbf{n}_m$.

(G) Polarizing optical microscopy image of the microrod dispersion, as viewed between the crossed polarizer (P) and analyzer (A).

To ensure dense dispersions of the microrods in 5CB, they are coated with perfluorocarbon molecules that are known to induce "slippery surface" weak anchoring effects[26,27] and produce weak perpendicular anchoring of nematic director/molecules,[28] aiding in dispersion by reducing the energetic costs of particle-induced director distortions. These LC-colloidal dispersions are then introduced into glass cells with dimensions of approximately 1.8 cm by 1.8 cm and gap thicknesses ranging from 10 to 60 μm. The inner surfaces of the cells are treated to define monodomain nematic LC samples, with the surfaces designed to establish either perpendicular or tangential boundary conditions for the molecular director $\mathbf{n}_m$. The nematic samples with rods are allowed to settle for several hours to reach the desired concentration of particles. Within a dilute dispersion, at room temperature, the surfaces of the porous and slippery microrods naturally exhibit weak planar boundary conditions for the molecular director $\mathbf{n}_m$ of a planar cell and align themselves parallel to it (see Figure 1F). These sample preparation conditions result in the induction of only weak elastic distortions of the molecular alignment around the porous microrods owing to the weak anchoring strength at LC-colloidal interfaces, contrasting with microparticles that induce bulk defects[11,12] but similar to a large variety of nanoparticles exhibiting soft surface boundary conditions,[29,30] as revealed by polarizing optical microscopy image of the dispersion in Figure 1G. This behavior arises from minimizing the overall free energy, where elastic distortions compete with the cost associated with deviations of $\mathbf{n}_m$ away from the weak locally perpendicular boundary conditions at the particles' surfaces. No strong deformations of the bulk LC director field were found because violating colloidal surface boundary conditions simply costs less energy than ones with strong director deformations in the nematic bulk. Although weak bulk elastic deformations around particles can still lead to elasticity-mediated anisotropic interparticle colloidal forces, including attractive ones, these forces can be overcome by purely repulsive electrostatic interactions associated with surface charging of the used particles, discussed below.

To monitor elastic-electrostatic interaction interplay while assuring colloidal stability, we probed the surface charge of individual microrods, finding it to be within a range $Z_e \approx -(100–250)e$, where *e* represents the elementary charge and *Z* corresponds to the number of effective elementary charges present on the microrods (see Figure S2). To characterize the colloidal rods' surface charging properties, we studied their electrophoretic mobility in response to an applied electric field. Using the balance of electrophoretic and the viscous drag forces, we obtain insights into the colloidal surface charging,[31,32] which allow us

Please cite this article in press as: Ghosh et al., Reconfigurable self-assembly of porous anisotropic colloids in nematic liquid crystals, Matter (2025), https://doi.org/10.1016/j.matt.2025.102563

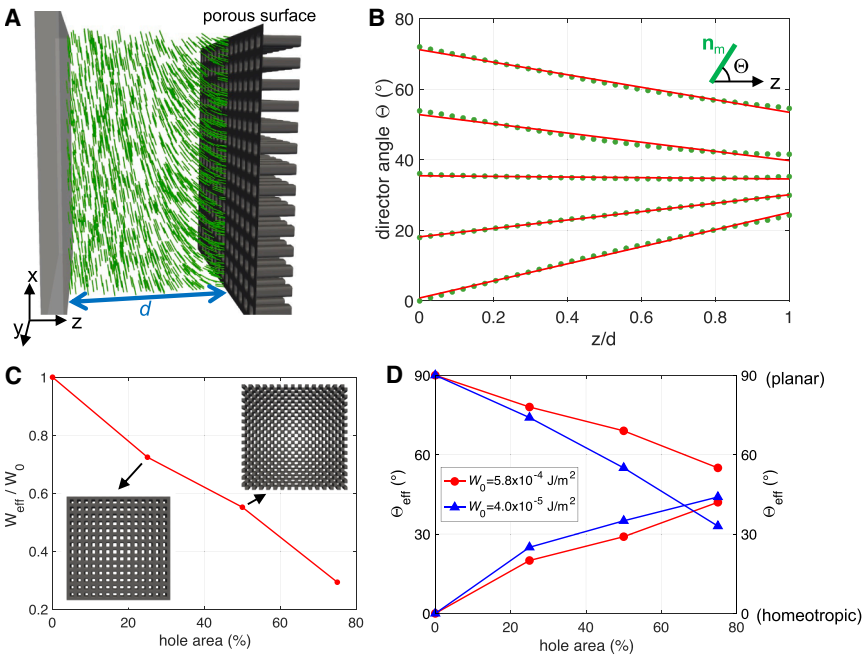

Figure 2. Effective surface anchoring of porous colloidal particles

(A) A schematic of a geometric configuration used to simulate the effective surface anchoring phenomenon, with the fixed boundary conditions at the left side and the other boundary being non-smooth. The LC director field is represented by green cylinders.

(B) Numerical equilibrium angles, defined as the angle made by director and *z* axis (inset), of LC directors (green) inside the hybrid cell and their linear fit (red lines). The 5 independent simulations are carried out with different angles at the fixed boundary (z = 0) but with the same porous surface (z = *d*).

(C) Numerical effective surface anchoring strengths for porous surfaces. The values are scaled by its value for a flat surface (hole area = 0). Insets show the front view of square-periodic porous surfaces having 25% and 50% hole area, respectively.

(D) Numerical effective surface anchoring cone angles (Θ_{eff}) for porous surfaces. For each set with connected dots, 0% hole area recovers local surface anchoring types, either Θ_{eff} = 0 (homeotropic) or Θ_{eff} = 90° (planar), and local surface strengths $W_0 = 5.8 \times 10^{-4}$ Jm^{-2} (red circles) or $W_0 = 4.0 \times 10^{-5}$ Jm^{-2} (blue triangles).

to control the interplay between electrostatic and elastic forces and avoid irreversible aggregates in dense colloidal dispersions.

Emergent weak anchoring boundary conditions of porous colloids

For colloidal dispersions with a low particle concentration, the behavior of individual microrods is dominated by colloidal-molecular interactions, i.e., the particles' surface anchoring effects, the anisotropic part of the surface energy that defines the boundary condition for the 5CB molecules and director at colloidal surfaces. As a result, the microrods choose their long-axis orientation $\mathbf{l}_c$ such that the sum of surface anchoring energy and the bulk energy of particle-induced elastic distortions in the director $\mathbf{n}_m$ is minimized. To understand our system's behavior at this level, we consider the energetic cost of LC's interaction with a surface containing an array of holes mimicking pores (Figure 2), while assuming that the system's energetics can be described in terms of the elastic energy of director distortions near the holes and the anchoring energy cost at the LC-particle interfaces (methods). Surface anchoring for the LC director at surfaces can be perpendicular (homeotropic, $\Theta_e = 0°$), tangentially degenerate (Θ_e = 90°), or conically degenerate anchoring ($0° < \Theta_e < 90°$), depending on the local equilibrium easy axis orientation angle Θ_e between the molecular director $\mathbf{n}_m$ and the local colloidal surface normal direction.[33] The energetic cost of deviating the director $\mathbf{n}_m$ away from the easy axis by an angle Θ_s can be quantified by the surface energy density f_{surf}:

$$f_{surf} = \frac{W_0}{2}\left(\cos^2(\Theta_s) - \cos^2(\Theta_e)\right)^2 \qquad \text{(Equation 1)}$$

where the surface anchoring coefficient W_0 is in units of energy per area. The conical degenerate surface energy potential, Equation 1, is commonly used in modeling LC on flat surfaces.[5,33,34] To describe our etched, porous surface we introduce an effective coarse-grained anchoring with parameters $W_0 = W_{eff}$ and $\Theta_e = \Theta_{eff}$ describing the effective model's coefficients for uneven porous surfaces (Figure 2). By considering surface topography with holes mimicking that of the etched particle surface after the alkaline treatment (Figure 2A), we numerically calculate the equilibrium configuration of $\mathbf{n}_m$ near the surface (Figure 2B). We then compute the associated effective parameters W_{eff} and Θ_{eff} for such porous surfaces by presenting the energetics of nematic-surface interactions in terms of the effective surface anchoring energy given by Equation 1 (see methods). As one could intuitively anticipate, we find that the magnitude of W_{eff} decreases with an increase in the hole area dependent on the particle's porosity (Figure 2C). Interestingly, we also discover that porous surfaces tend to exhibit generally conical effective surface anchoring with Θ_{eff} giving intermediate angles depending on the topography details, for which local surface anchoring types can be both tangential and perpendicular (Figure 2D). This effective conical anchoring angle Θ_{eff} is naturally related to the distribution of tilting of the local surface normals of the porous particle's surface.

By using the ensuing effective anchoring parameters $W_0 = W_{eff}$ and $\Theta_e = \Theta_{eff}$, we then do numerical modeling at a larger scale via minimizing the energy due to overall colloidal inclusions in a nematic host, as we previously described in Mundoor et al.[5] This process reveals how each anisotropic colloidal particle interacts with the nematic host at different temperatures and finds equilibrium orientation that minimizes the LC surface energy[5] as well as the bulk elastic energy due to weak particle-induced deformations of director (Figures 3A and 3B).

Please cite this article in press as: Ghosh et al., Reconfigurable self-assembly of porous anisotropic colloids in nematic liquid crystals, Matter (2025), https://doi.org/10.1016/j.matt.2025.102563

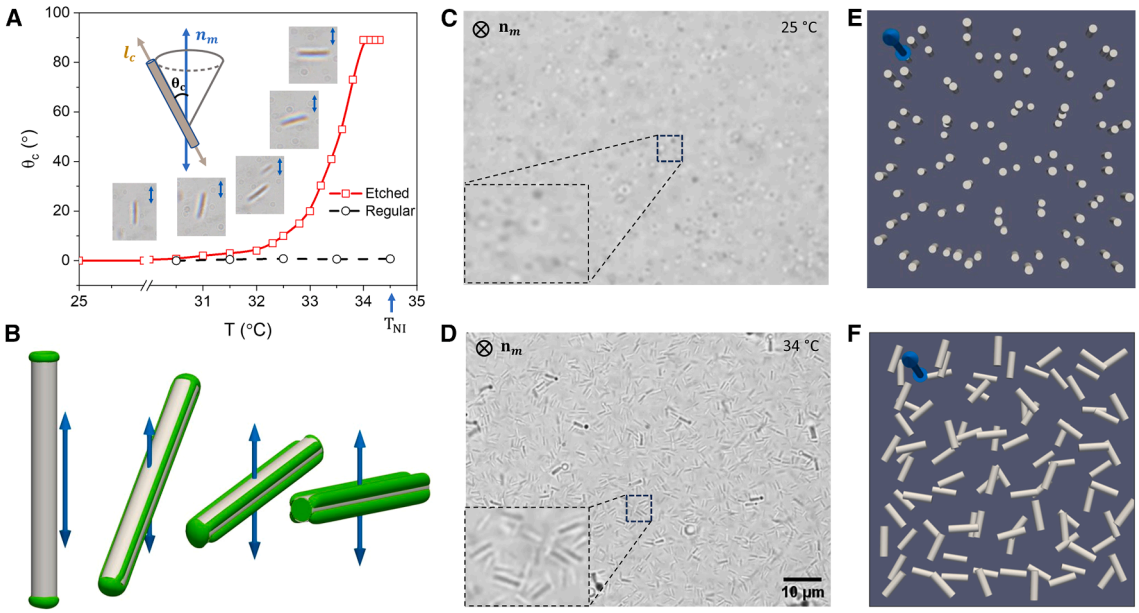

Figure 3. Thermally reconfigurable surface anchoring of porous colloidal particles

(A) Angle θ_c between the molecular director $\mathbf{n}_m$ and colloidal long axis $\mathbf{l}_c$, as defined in the top-left inset, versus temperature (T) for regular and etched rods. Other insets along the red curve show bright-field micrographs with different microrod orientations.

(B) Numerically simulated $\mathbf{n_m}$ distortions (green) induced by coarse-grained porous rods with various equilibrium θ_c, each with energy-minimizing surface anchoring cone angle Θ_{eff} (see methods). $W_{eff} = 10^{-5}$ Jm^{-2} for all cases. Green iso-surfaces depict spatial regions where local $\mathbf{n_m}$ deviates away from the far-field orientation of $\mathbf{n_m}$.

(C and D) Bright-field micrographs of collective dispersion of colloids in a homeotropic cell aligned along $\mathbf{n}_m$ at room temperature and reorienting perpendicular to $\mathbf{n}_m$ at temperatures above 34°C.

(E and F) Schematic visualization of the nematic phases in (C) and (D), respectively, with the porous rods represented by gray cylinders and $\mathbf{n}_m$ parallel to the viewing direction.

Thermal reconfiguration of orientation and diffusive properties of microrods

In our experiments, the porosity of rods suppresses the energy penalty of spontaneous fluctuation in the microrod's orientation direction due to lowering W_{eff}. The porous "slippery" microrods within the nematic dispersion exhibit thermally reconfigurable surface boundary conditions at temperatures below nematic-isotropic transition, which is found to be $T_{NI} \approx 34.5°C$ for the 5CB-based hybrid fluid (approximately 1°C below the $T_{NI}$of the pristine 5CB compound). In a planar cell, the porous microrods are found to spontaneously rotate relative to $\mathbf{n}_m$ with increasing temperature, eventually aligning perpendicular to it, with the orientations quantified by angles θ (Figures 3A and 3B). This behavior is different from that of nonporous rods with the same slippery surface functionalization obtained by otherwise similar preparation methods, which do not exhibit temperature-driven reorientation. The thermal reorientation of $\mathbf{l}_c$ of porous rods arises from reconfigurable surface boundary conditions due to the interplay between electrostatic[32] and conventional temperature-dependent molecular interactions[34] at the porous colloidal surfaces, which yields a well-defined energetic minimum and a narrow orientational distribution of $\mathbf{l}_c$ at each temperature. The rotation of the microrod axis $\mathbf{l}_c$ leads to changes of the effective symmetry of the nematic colloidal building blocks. A similar reorienting behavior is also observed when the porous microrods are coated with other surfactants, like DMOAP. However, in the latter case, the thermal reconfiguration of the colloidal rods happens over a broader temperature window (as shown in Figure S3). These DMOAP-capped porous particles are initially parallel to $\mathbf{n}_m$ at room temperature, then undergo thermally driven reconfiguration, and finally align perpendicular to $\mathbf{n}_m$ at temperatures above 34°C (Figures 3C–3F). This behavior differs from that of nonporous microrods with DMOAP coating showing no thermal dependence of orientational distributions despite aligning perpendicular to $\mathbf{n}_m$ at room temperature. In dilute dispersions with $\mathbf{l}_c$ of rods perpendicular to $\mathbf{n}_m$, thermal fluctuations also freely rotate microrods around $\mathbf{n}_m$ while maintaining the overall uniaxial $D_{\infty h}$ symmetry of the overall nematic colloidal dispersion, similar to that of the rod-shaped molecules of the 5CB nematic host medium.

Colloidal microrods with temperature-dependent surface boundary conditions experience orientation-dependent viscous drag acting on the particles accompanied by weak induced director distortions (Figure 3B), resulting in different anisotropic diffusion at different temperatures.[35] We determine the diffusion coefficients by employing video microscopy tracking of the rod's position.[23,24,36] The anisotropic translational diffusion (Figures 4A and 4B) is the most pronounced for particles with tangential effective surface anchoring. For perpendicular anchoring, the polar plot of D_t is effectively (and qualitatively) rotated with respect to both $\mathbf{n}_m$ and $\mathbf{l}_c$, with a typical angle between $\mathbf{l}_c$ and the maximum displacement direction being about

Please cite this article in press as: Ghosh et al., Reconfigurable self-assembly of porous anisotropic colloids in nematic liquid crystals, Matter (2025), https://doi.org/10.1016/j.matt.2025.102563

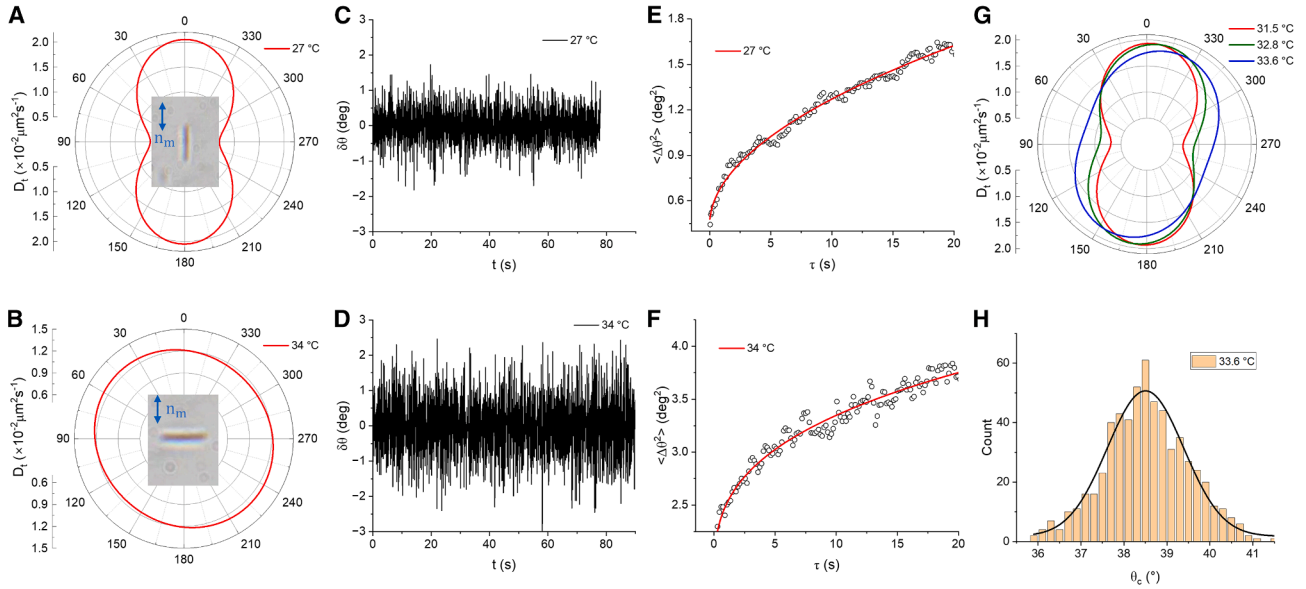

Figure 4. Characterization of translational and rotational diffusion of microrods

(A) Translational diffusion of microrods with planar surface boundary condition in planar cell of nematic LC.

(B) Translational diffusion of microrods with perpendicular surface boundary condition in planar cell of nematic LC.

(C and D) Orientational fluctuations $\delta\theta$ versus time (t) obtained at τ = 67 ms, of a microrod when $\mathbf{l}_c \| \mathbf{n}_m$ and $\mathbf{l}_c \perp \mathbf{n}_m$.

(E and F) Angular mean square displacement $\langle \Delta\theta^2 \rangle$ versus lag time (τ) in a planar cell for microrods with planar and perpendicular anchoring, respectively. A solid red line is a fit of experimental data (black circles).

(G) Translational diffusion of microrods with conical surface boundary condition at three different temperatures in planar cell of nematic LC.

(H) Histogram of microrods orientations obtained at τ = 67 ms during T = 33.6°C.

45°. Furthermore, the microrods undergo rotational diffusion, where they tilt away from the energy-minimizing orientation of the colloidal rod's long axis $\mathbf{l}_c$ by an angular displacement $\delta\theta = \theta - \theta_c$, in addition to rotating around the θ_c-cone at low number densities of microrods. The effective angular displacement $\delta\theta$ of microrods with perpendicular boundary conditions at 34°C is greater than that of ones with tangential boundary conditions at 27°C (see Figures 4C and 4D); the corresponding rotational diffusion coefficients are $D_r \approx 3.71$ deg^{2}s^{-1} and ≈ 10.44 deg^{2}s^{-1} at 27°C and 34°C, respectively. Figures 4E and 4F shows the rotational mean square displacement (MSD) $\langle \Delta\theta^2 \rangle$ of the microrods with the two types of effective anchoring versus the lag time τ. For both orientations, the $\langle \Delta\theta^2 \rangle$ initially increases and then starts to saturate, indicating subdiffusive behavior attributed to the LC-related anchoring and elastic forces. However, the angular MSDs of rods with perpendicular anchoring are higher than those of the rods with tangential surface anchoring. At intermediate temperatures (~31.5°C–34°C) the conical anchoring and tilting of microrods reduce diffusion anisotropy with increasing temperature, as shown in Figure 4G. For a given selected temperature of 33.6°C, Figure 4H shows a typical histogram of the variation in θ, which corresponds to an average orientation at θ_c = 38.5°. The typical angle between equilibrium orientation of $\mathbf{l}_c$ and the direction of its maximum displacement is about 15°, varying between 10° and 20°, depending on temperature.

The above characterizations reveal thermally reconfigurable colloidal building blocks comprising microrod particles with coronae of weakly distorted molecular ordering in a nematic host medium. With anisotropic properties featured at both molecular and colloidal scales, an intruding question arises: what types of condensed matter phases can emerge from the self-assembly of such building blocks?

Emergent phase behavior of hybrid molecular-colloidal liquid crystal system

Colloidal particles at different equilibrium orientations θ_c cause perturbations in the director field (Figure 3B), associated with the elastic free energy costs, which, in turn, give origins to tunable anisotropic interactions at their different temperature-dependent orientations. By harnessing this temperature-dependent interplay of surface anchoring and elastic effects, we achieve diverse behaviors in our hybrid molecular-colloidal system (Figures 5 and 6). The ensuing nematic colloidal configurations are explored while varying temperature and particle concentration. Increasing the microrod number density per unit volume ρ first decorates the molecular director $\mathbf{n}_m$ with progressively denser dispersions of colloidal microrods collinear with it, defining the colloidal director $\mathbf{n}_c$ of overall uniaxial molecular-colloidal hybrid nematic LC, where colloidal orientational distributions somewhat vary with temperature (Figures 5A and 5B). At higher densities, intercolloidal interactions cause emergence of local smectic-like quasi-one-dimensional correlations (Figure 5C), somewhat reminiscent of cybotactic clusters found in conventional molecular LCs.[37] By using phase-contrast imaging, we probe these quasi-one-dimensional positional correlations, as well as the corresponding transmitted-light intensity

Please cite this article in press as: Ghosh et al., Reconfigurable self-assembly of porous anisotropic colloids in nematic liquid crystals, Matter (2025), https://doi.org/10.1016/j.matt.2025.102563

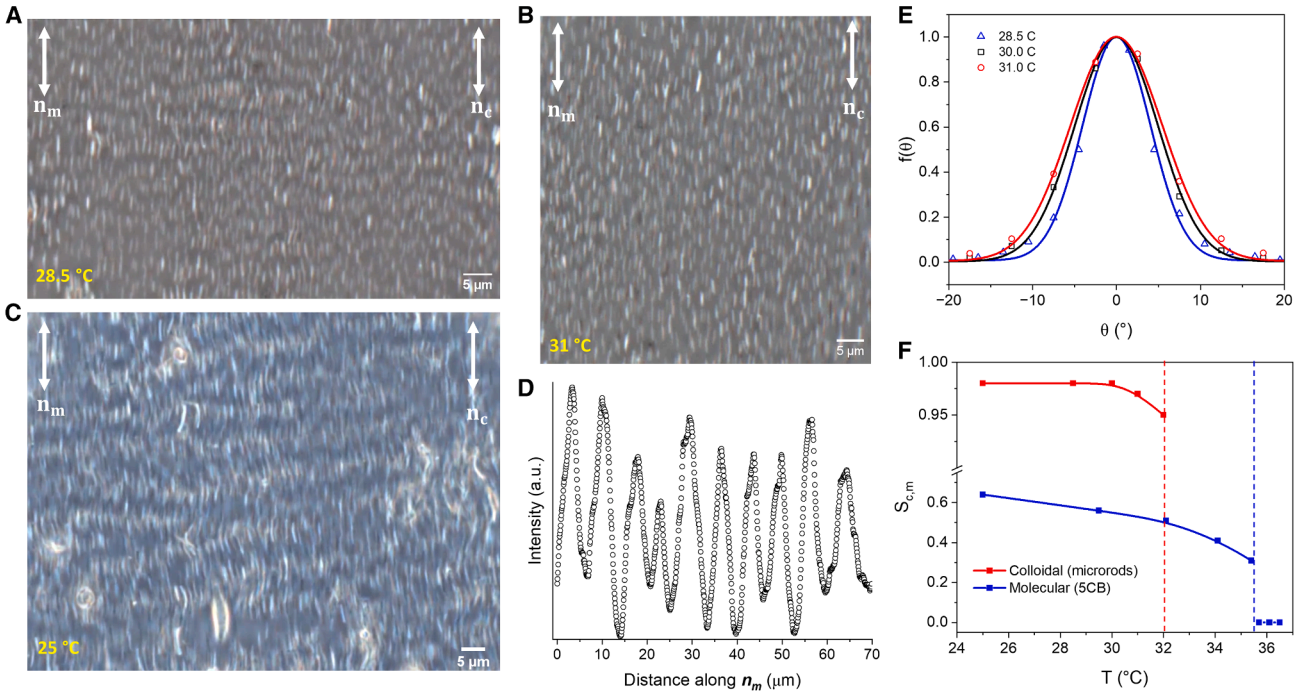

Figure 5. Self-assembly of microrods with planar surface boundary conditions

(A and B) Phase-contrast micrograph of colloidal dispersion at elevated temperatures exhibiting dissociation of colloidal layers and (B) transforming into uniaxial molecular-colloidal nematic fluid without any positional correlations.

(C) Phase-contrast micrograph of colloidal dispersion colinear with $\mathbf{n}_m$ showing cybotactic phase with short range one-dimensional ordering.

(D) Intensity variation along $\mathbf{n}_m$ in (C) confirming the formation of quasi-layered colloidal structures with short-range positional correlations. Areas without the colloidal layer appear darker in phase-contrast imaging.

(E) Distribution of θ_c at $\rho = 0.2$ for 28.5°C (blue triangles), 30°C (black squares), and 31°C (red circles).

(F) Uniaxiality order parameter $S_{c,m}$ versus T for colloids characterized by video tracking and for pure 5CB (for reference) characterized by Raman spectroscopy previously.[6] The blue dashed line indicates the nematic-isotropic transition temperature for pure 5CB,[38] and the red dashed line indicates the planar-conical anchoring transition temperature of the colloidal microrods.

variations when probed along $\mathbf{n}_c$ (see Figure 5D), across the "quasi-layers" of particles. From such experiments we find an average interlayer separation of d = 3.35 ± 0.48 µm. As the temperature increases, the smectic-like quasi-layering gradually diminishes, and the system then again exhibits a uniaxial quasi-layer correlations-free molecular-colloidal nematic phase, as depicted in Figure 5B.

We analyze the orientational distribution function (f_c) as a means of quantifying the probabilities of different orientations of colloids in the nematic phase, finding that f_c broadens with increasing temperature. Using the experimental f_c data, we determine the orientational order parameters associated with the colloidal rods, such as the scalar order parameter S_c. Figure 5F shows S_c value close to 1 at room temperature, corresponding to the uniaxial ordering of colloids with the colloidal director $\mathbf{n}_c$ along $\mathbf{n}_m$ and with the degree of alignment S_c higher than that of the molecular host LC itself. Subsequently, as the temperature of the system is increased beyond 31°C, the microrods start tilting away from $\mathbf{n}_m$ (Figures 6A and 6B). The orientational distribution of microrods (see Figure 6C) reflects the increase in θ_c with temperature, consistent with the thermal behavior of individual particles (Figure 3A). The microrods finally become orthogonal to $\mathbf{n}_m$ at temperatures above 34°C due to perpendicular effective anchoring at such temperatures. While in dilute dispersions thermal fluctuations rotate microrods around $\mathbf{n}_m$ (Figures 6D and 6E), thereby still maintaining the uniaxial $D_{\infty h}$ symmetry of the hybrid nematic molecular-colloidal LC,[39] increasing particle density leads to more complex, emergent effects.

The increase of particle concentration to values $\rho > 0.2$ leads to a transition from a uniaxial to a low-symmetry hybrid nematic phase, which is orthorhombic at temperatures above 34°C. The emergent collective orientational order of the microrods defines a nonpolar colloidal director $\mathbf{n}_c$ that is orthogonal to $\mathbf{n}_m$. In a cell where in-plane $\mathbf{n}_m$ is parallel to substrates, $\mathbf{n}_c$ spontaneously aligns perpendicular to $\mathbf{n}_m$, while also being parallel to the substrates, resulting in an orthorhombic biaxial molecular-colloidal nematic phase (Figures 6H and 6I). Thus, the biaxial D_{2h} orthorhombic symmetry of this molecular-colloidal nematic LC is characterized by three directors,[6,38] $\mathbf{n}_m$, $\mathbf{n}_c$, and $\mathbf{n}_\perp$, of which the third is orthogonal to both $\mathbf{n}_m$ and $\mathbf{n}_c$. Although a small fraction of microrods is found misaligned, e.g., pointing along $\mathbf{n}_\perp$, this fraction reduces significantly at higher ρ, yielding a narrow azimuthal width of colloidal orientations, $f_c(\theta)$ (Figure 6K). Unlike conventional phase transitions where increasing temperature leads to progressive melting of ordered states toward disorder,

Please cite this article in press as: Ghosh et al., Reconfigurable self-assembly of porous anisotropic colloids in nematic liquid crystals, Matter (2025), https://doi.org/10.1016/j.matt.2025.102563

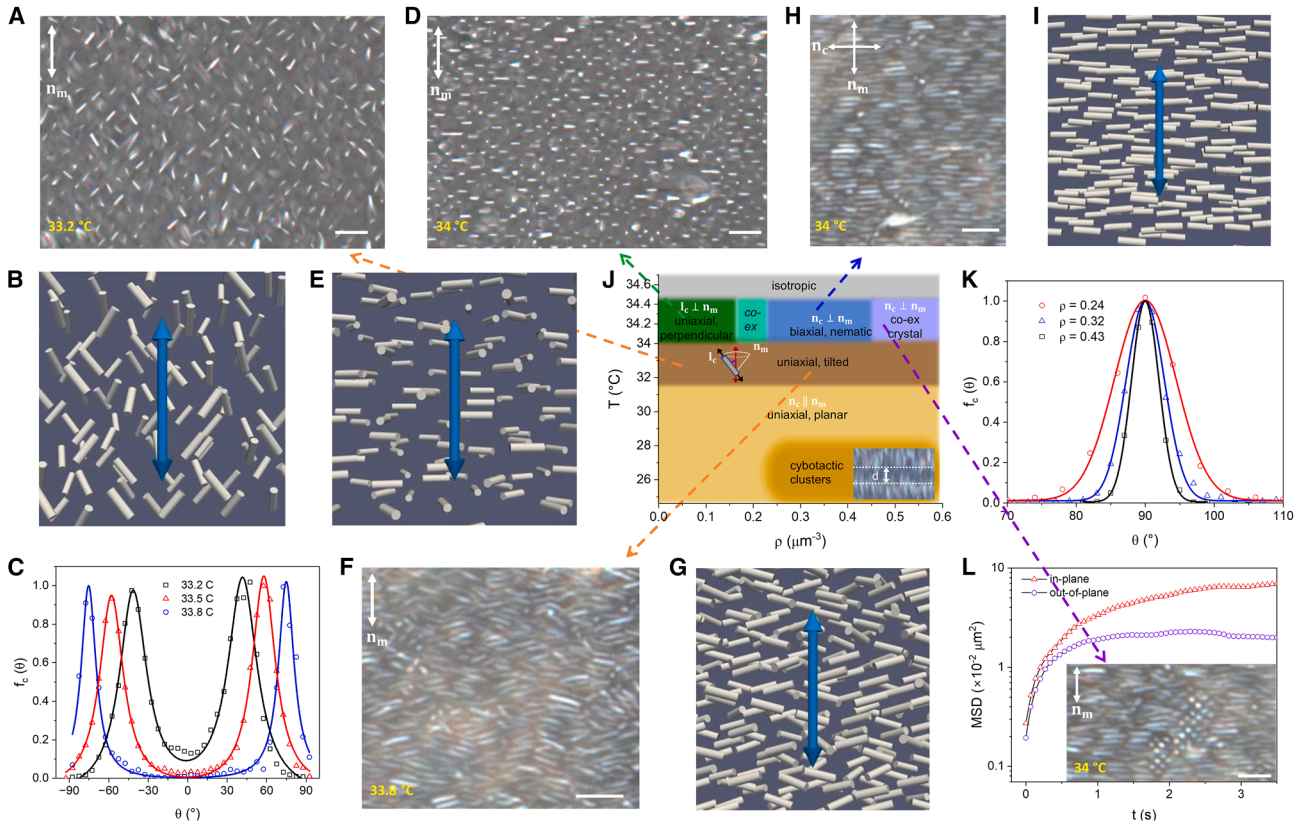

Figure 6. Concentration and temperature-dependent phase behavior of colloidal-LC dispersions

(A) Phase-contrast micrographs of colloidal dispersion tilted with respect to $\mathbf{n}_m$ displaying conical anchoring at $\rho = 0.15$ and $T = 33.2°C$.

(B) Schematic visualization of the nematic phase in (A), with the porous rods represented by gray cylinders and $\mathbf{n}_m$ represented by blue double arrow.

(C) $f_c(\theta)$ versus θ at different T values for particle tilting away from $\mathbf{n}_m$.

(D) Phase-contrast micrographs of colloidal dispersion displaying perpendicular anchoring at $\rho = 0.15$ and $T = 34°C$.

(E) Schematic visualization of the nematic phase in (D); $\mathbf{n}_m$ represented by blue double arrow.

(F) Phase-contrast micrographs of colloidal dispersion tilted with respect to $\mathbf{n}_m$ displaying conical anchoring at $\rho = 0.43$ and $T = 33.8°C$.

(G) Schematic visualization of the nematic phase in (F); $\mathbf{n}_m$ represented by blue double arrow.

(H) Phase-contrast micrographs of microrods in a biaxial hybrid LC showing their alignment along colloidal director $\mathbf{n}_c$, orthogonal to $\mathbf{n}_m$.

(I) Schematic visualization of the nematic phase in (H); $\mathbf{n}_m$ represented by blue double arrow.

(J) Phase diagram of the hybrid molecular-colloidal system exhibiting uniaxial nematic, isotropic, cybotactic, biaxial nematic, and coexisting crystal-nematic phases. The optical microscopic image in the inset shows the two layers of cybotactic clusters with an interlayer separation (d). The schematic shows tilted orientation of the colloids with respect to the molecular director.

(K) $f_c(\theta)$ versus θ at $T = 34°C$ and $\rho = 0.24$ (red circles), 0.32 (blue triangles) and 0.43 (black squares).

(L) MSDs of microrods over time t at $T = 34°C$ and at $\rho = 0.56\ \mu m^{-2}$ for particles oriented along $\mathbf{n}_c$ (red triangles) and for particles oriented along $\mathbf{n}_\perp$ (purple circles), which is orthogonal to both $\mathbf{n}_c$ and $\mathbf{n}_m$. The inset shows the phase-contrast image of colloidal crystal assembly of microrods oriented along $\mathbf{n}_\perp$ and nematic assembly of colloids oriented along $\mathbf{n}_c$, coexisting at $T = 34°C$.

Scale bars, 5 μm.

surprisingly, here we observe the formation of a more ordered, lower-symmetry orthorhombic nematic phase as we heat up the uniaxial system with a concentrated colloidal dispersion, distantly resembling molecular-colloidal system with disk-shaped particles.[5] This phenomenon emerges within an equilibrium setting due to symmetry-breaking caused by changes in the coupling between the molecular LC host and colloidal surfaces, as well as the interplay of elastic, electrostatic, and steric interactions.

In addition to the biaxial and uniaxial hybrid molecular-colloidal nematic states, as well as pre-transitional effects like the cybotactic clusters, the temperature-concentration phase diagram exhibits isotropic as well as biphasic regions, where different states co-exist (Figure 6J). The two-phase coexistence regions appear at the uniaxial-biaxial transitions and at high-T, high-ρ conditions. At high concentration values $\rho > 0.42$ and when homeotropic anchoring is dominant, microrods pointing along $\mathbf{n}_\perp$ tend to form two-dimensional crystalline domains co-existing with the orthorhombic biaxial nematic phase[31] (Figures 6J–6L). To reveal the system's fluidity and dynamics of the microrods, in Figure 6L we show the two-dimensional MSD $\langle \Delta r^2 \rangle$ versus time (t) for particles aligned in-plane (along $\mathbf{n}_c$) and out-of-plane (along $\mathbf{n}_\perp$ orthogonally to the glass substrate). We find that the microrods aligned out of plane,

Please cite this article in press as: Ghosh et al., Reconfigurable self-assembly of porous anisotropic colloids in nematic liquid crystals, Matter (2025), https://doi.org/10.1016/j.matt.2025.102563

orthogonally to the substrate, tend to assemble into periodic lattices of crystallites, indicating the local emergence of crystalline order. On the other hand, the microrods aligned in-plane with the substrate remain in a fluid-like state exhibiting orientational order but no positional correlations (see inset of Figure 6L). The behavior of these colloidal crystallites co-existing with the surrounding hybrid molecular-colloidal biaxial nematic medium stems from balancing of repulsive electrostatic and anisotropic elasticity-mediated interactions due to distortions in the host LC's molecular order around the rods.

Modeling of low-symmetry nematic phases of the hybrid molecular-colloidal system

To get insights into the large-scale molecular-colloidal self-assembly of low-symmetry hybrid nematic LC phases, it is instructive to consider the coarse-grained view of the system where colloidal rods are assumed to have infinitely strong coupling of orientations at temperature-dependent θ_c angles to the $\mathbf{n}_m$ director of the molecular host medium. The interplay between bulk, elastic, and surface interactions is responsible for the self-assembly in hybrid molecular liquid crystalline-colloidal systems. By varying temperature and colloid concentration, these systems exhibit a series of symmetry reduction transitions, progressing from isotropic (I) through uniaxial nematic (N), orthorhombic biaxial nematic (N_{ob}), to monoclinic biaxial nematic (N_{mb}) phases. As temperature and colloid concentration are the laboratory-controlled parameters responsible for these ordered nematic phases, the corresponding sequence of global symmetry breaking can also be characterized at the length scale of colloidal ordering, which we refer to as infinite anchoring extrapolation length limit. At this scale, to the leading order, the local molecular and colloidal directors can be approximated by their sample-averaged mean directions, disregarding weak distortions of molecular order depicted in Figure 3B. From this perspective, the nematic phases exhibited by these hybrid systems can be viewed as if they were spatially homogeneous, undergoing symmetry reduction consistent with Landau-de Gennes theory of nematics. Here, we will examine some of the consequences of the above assumption.

In the conventional description of ordinary nematics, given the absence of polarity and chirality, we typically introduce a 3×3 spatially independent symmetric and traceless alignment tensor $\mathbf{Q_m}$, with components $Q_{m,\alpha\beta}$, to quantify the emerging global orientational order (see, e.g., Selinger,[40] Gramsberger et al.,[41] and Allender and Longa[42]). When dealing with two-component systems consisting of an LC host such as 5CB mesogens and colloids, where the pure systems can only stabilize an ordinary uniaxial nematic phase, we need at least two alignment tensors: $\mathbf{Q_m}$ for the liquid crystalline component and $\mathbf{Q_c}$ for the colloidal component. In this section, we will explore some implications of this approach, specifically addressing the aforementioned symmetry reduction in nematics.

To account for the reduction in symmetry from isotropic to ordinary uniaxial nematic, we usually start with the Landau-de Gennes expansion in terms of the alignment tensor, which in our case would involve an *O(3)*-invariant expansion of the nonequilibrium free energy $F[\mathbf{Q}_m, \mathbf{Q}_c]$ in powers of the order parameters $\mathbf{Q}_m$ and $\mathbf{Q}_c$. Coarse-graining to the colloidal length scale allows us to neglect gradient and surface terms; temperature-density dependent anchoring between LC molecules and colloids is effectively managed by the bulk couplings that facilitate the mutual orientation of the global directors. This expansion must be invariant with respect to the symmetry operations of the *O*(3)-symmetric disordered liquid state, where $\mathbf{Q}_m = \mathbf{Q}_c = \mathbf{0}$. The only restrictions on $F[\mathbf{Q}_m, \mathbf{Q}_c]$ are that it must be analytical in $\mathbf{Q}$s and stable against an unlimited growth of $\mathbf{Q}$s. The free energy of the combined system is then a polynomial expansion in terms of the invariants constructed out of tensors $\mathbf{Q}_m$ and $\mathbf{Q}_c$. It involves the free energy of the molecular subsystem ($F_m[\mathbf{Q}_m]$) and the colloidal subsystem ($F_c[\mathbf{Q}_c]$) and the coupling between the two subsystems ($F_{mc}[\mathbf{Q}_{mc}, \mathbf{Q}_m, \mathbf{Q}_c]$). The expansion, complete up to the fourth order in $\mathbf{Q}$s, reads[43,44]

$$F[\mathrm{Q_m}, \mathrm{Q_c}] = F_m[\mathrm{Q_m}] + F_c[\mathrm{Q_c}] + F_{mc}[\mathrm{Q_{mc}}, \mathrm{Q_m}, \mathrm{Q_c}],$$

$$F_m[\mathrm{Q_m}] = a_m \,\mathrm{Tr}\left(\mathbf{Q_m^2}\right) - b_m \mathrm{Tr}\left(\mathbf{Q_m^3}\right) + \mathrm{Tr}\left(\mathbf{Q_m^2}\right)^2,$$

$$F_c[\mathrm{Q_c}] = -a_c \,\mathrm{Tr}\left(\mathbf{Q_c^2}\right) - b_c \mathrm{Tr}\left(\mathbf{Q_c^3}\right) + \mathrm{Tr}\left(\mathbf{Q_c^2}\right)^2,$$

$$\begin{aligned} F_m[\mathrm{Q_{mc}}, \mathrm{Q_m}, \mathrm{Q_c}] &= \lambda_2 \,\mathrm{Tr}(\mathbf{Q_{mc}}) + \lambda_{31} \,\mathrm{Tr}(\mathbf{Q_m Q_{mc}}) \\ &+ \lambda_{32} \,\mathrm{Tr}(\mathbf{Q_{mc} Q_c}) + \mathrm{Tr}\left(\mathbf{Q_m^2}\right)\mathrm{Tr}\left(\mathbf{Q_c^2}\right) \\ &+ \lambda_{41} \mathrm{Tr}\left(\mathbf{Q_m^2}\right)\mathrm{Tr}(\mathbf{Q_{mc}}) + \lambda_{42} \mathrm{Tr}\left(\mathbf{Q_c^2}\right)\mathrm{Tr}(\mathbf{Q_{mc}}) \\ &+ \lambda_{22} \,\mathrm{Tr}(\mathbf{Q_{mc}})^2 + \lambda_4 \mathrm{Tr}\left(\mathbf{Q_{mc}}^T \mathbf{Q_{mc}}\right) \end{aligned} \quad \text{(Equation 2)}$$

where $(\mathrm{Q_{mc}})_{\alpha\beta} = \mathrm{Q_{mc,\alpha\beta}} = \mathrm{Q_{m,\alpha\gamma}} \mathrm{Q_{c,\gamma\beta}}$ and the superscript "*T*" denotes transposed matrix and Tr denotes trace, the sum of diagonal elements of the matrix. Additionally, unless otherwise specified, summation is implied on repeated Greek indices.

According to the assumptions of Landau theory, we take $a_m = a_{m,0}(T - T_0)$ and $a_c = a_{c,0}(\rho - \rho_0)$, where T is the temperature (the leading control parameter for the molecular part) and ρ is the density of microrods (the leading control parameter for the colloidal part). The rest of the coefficients are assumed to be constant, with three redundant ones set to one. The minimal coupling expansions for separate molecular and colloidal parts depend on the structures that are stabilized for pure subsystems. In Equation 2, we assumed that pure systems form at most the uniaxial nematic phases, i.e., they are described by terms up to the fourth-order expansion in $\mathbf{Q}$s (see Allender and Longa[42]). The symmetry of the combined structures is governed by tensors $\mathbf{Q_m}$, $\mathbf{Q_c}$, and $\mathbf{Q_{mc}}$. When $F_{mc} = 0$, the resulting free energy F represents a degenerate case where the molecular and microrod subsystems decouple. This decoupling implies that the mutual orientations of the averaged directors of $\mathbf{Q}$s are not fixed relative to each other, and the equilibrium structures available from the expansion Equation 2 are *I* and *N*, independently for each subsystem. The presence of coupling terms fixes the relative orientation of the directors, with a nonzero value of $\mathbf{Q_m}$ implying a nonzero value of $\mathbf{Q_c}$, and vice-versa.

The equilibrium structures resulting from the minimization of Equation 2 can be illustrated by considering the exemplary forms

Please cite this article in press as: Ghosh et al., Reconfigurable self-assembly of porous anisotropic colloids in nematic liquid crystals, Matter (2025), https://doi.org/10.1016/j.matt.2025.102563

of the tensors $\mathbf{Q_m}$ and $\mathbf{Q_c}$. Assuming (1) the director of $\mathbf{Q_m}$ is oriented along the *z* axis of the laboratory frame of reference, (2) the biaxiality of $\mathbf{Q_m}$ is negligible, and (3) the symmetry axis of the lowest symmetry phase—the monoclinic one—is along the *x* axis, we can write **Q**s as:

$$\mathbf{Q_m} = \begin{pmatrix} -S_m & 0 & 0 \\ 0 & -S_m & 0 \\ 0 & 0 & 2S_m \end{pmatrix},$$
$$\mathbf{Q_c} = \begin{pmatrix} 2(p_c - S_c) & 0 & 0 \\ 0 & S_c - p_c - S\cos(2\theta) & -S\sin(2\theta) \\ 0 & -S\sin(2\theta) & S_c - p_c + S\cos(2\theta) \end{pmatrix}, \quad \text{(Equation 3)}$$

where the directors of $\mathbf{Q_c}$ are given by an orthonormal right-handed tripod of vectors *{1,0,0}, {0,cosθ,sinθ}, {0,−sinθ,cosθ}*. This corresponds to a rotation of the laboratory frame by an angle θ about *x* axis, with $S = 3S_c + p_c$. For **Q**s given by Equation 3 and subject to $S_m \neq 0$, the corresponding $\mathbf{Q_{mc}}$ matrix is symmetric and diagonal if $S\sin(2\theta) = 0$ and nonsymmetric if $S\sin(2\theta) \neq 0$. In the former case, only uniaxial and biaxial nematic phases are stabilized, whereas in the latter case, the monoclinic nematic phase can be the equilibrium phase. For example, by setting $b_m = b_c = \lambda_2 = \lambda_{31} = \lambda_{32} = -\lambda_4 = -1$ and all the remaining parameters to zero, we find that for a fixed colloid density (e.g., $a_c = 1.5$) and low temperatures (e.g., $a_m = -3$), the equilibrium $\mathbf{Q_{mc}}$ is a uniaxial tensor. As the temperature increases, it transforms into a biaxial tensor and remains biaxial over a range of temperatures, consistent with experimental observations (see Figure 6). At even higher temperatures, $\mathbf{Q_{mc}}$ reverts to a uniaxial form. By fixing the temperature and increasing the density, we observe I-N and I-N-N_{ob}-N phase transitions.

For $0 < \theta < \pi/2$, we can stabilize the monoclinic biaxial nematic phase, which manifests as a nonzero antisymmetric part of the matrix $\mathbf{Q_{mc}}$. Equivalently, the appearance of monoclinic order can be quantified using the pseudovector order parameter $P_\alpha = \frac{1}{2}\ \epsilon_{\alpha\beta\gamma}\, Q_{mc.\beta\gamma} = \left\{\frac{3}{2}\, S_m S \sin(2\theta), 0, 0\right\}_\alpha$ along the symmetry axis of $\mathbf{Q_{mc}}$. As an example, we performed numerical minimization of Equation 2 with $b_m = b_c = \lambda_2 = \lambda_{22} = \lambda_4 = 1, \lambda_{31} = \lambda_{32} = -2$, and with the remaining parameters set to zero, obtaining phase sequences similar to the previous biaxial nematic example, except that the N_{ob} phase is replaced by the N_{mb} phase.

Finally, it should be noted that the free energy given by Equation 2 remains invariant under the following transformations:

$$\{\mathbf{Q_m}, \mathbf{Q_c}, b_m, b_c, \lambda_2, \lambda_{31}, \lambda_{32}, \lambda_{41}, \lambda_{42}\} \rightarrow$$
$$\{\{-\mathbf{Q_m}, \mathbf{Q_c}, -b_m, b_c, -\lambda_2, \lambda_{31}, -\lambda_{32}, -\lambda_{41}, -\lambda_{42}\},$$
$$\{\mathbf{Q_m}, -\mathbf{Q_c}, b_m, -b_c, -\lambda_2, -\lambda_{31}, \lambda_{32}, -\lambda_{41}, -\lambda_{42}\},$$

$\{-\mathbf{Q_m}, -\mathbf{Q_c}, -b_m, -b_c, \lambda_2, -\lambda_{31}, -\lambda_{32}, \lambda_{41}, \lambda_{42}\}\}$. This implies that for a given temperature and density and for fixed absolute values of the model parameters, there exists four equilibrium states $\{\pm\mathbf{Q_m}, \pm\mathbf{Q_c}\}$, achievable by changing the sign of the respective coefficients.[42] The sign choice for the examples given corresponds to the prolate symmetry of the $\mathbf{Q_{mc}}$ tensor in the N phase. A comprehensible spectrum of predictions from theory, Equation 2, along with experimental verification, will be addressed in a future publication.

DISCUSSION

With increased number density of freely diffusing nematic colloidal building blocks within an aligned 5CB host, the dense colloidal dispersions are observed causing only slight perturbations in the local molecular order (Figure 3B). Both polarizing optical microscopy and numerical modeling consistently reveal minimal disturbances to the nematic order surrounding the microrods with effectively soft boundary conditions arising from the porous nature of rods. Remarkably, within this system, we observe a variety of hybrid molecular-colloidal phases, which can be summarized with the help of phase diagram shown in Figure 6. These phases include nematic hybrid molecular-colloidal LCs with both uniaxial and biaxial symmetries, diagram regions with cybotactic clusters exhibiting short-range smectic-like ordering, and the emergence of crystallites coexisting with the fluid states of colloidal order and featuring two-dimensional positional correlations. Notably, all these emergent states exist within a single system comprising rod-like building blocks, with both molecular and colloidal rods characterized by uniaxial symmetry on their own. The diversity of this phase behavior can be understood by the formation of emergent low-symmetry building blocks via the oblique or orthogonal orientations of the molecular and colloidal rods, with the local C_{2h} or D_{2h} symmetries of the rod-like particles immersed in an aligned LC medium. Interestingly, the experimentally observed phase sequence can be also explained by the Landau-de Gennes theory incorporating two alignment tensors. In particular, the local D_{2h} blocks formed by orthogonal molecular and colloidal rods can self-organize to form the orthorhombic biaxial nematic phase, which can be monitored by, e.g., the symmetric part of the $\mathbf{Q_{mc}}$ tensor. Similarly, the presence of a nonzero antisymmetric part of $\mathbf{Q_{mc}}$ (equivalently of pseudovector $\boldsymbol{P}$) indicates the emergence of orientational order with C_{2h} symmetry, characterizing the monoclinic nematic phase of the composite materials.

Please cite this article in press as: Ghosh et al., Reconfigurable self-assembly of porous anisotropic colloids in nematic liquid crystals, Matter (2025), https://doi.org/10.1016/j.matt.2025.102563

Our findings also reveal that surface pores weaken anchoring boundary conditions and assist the self-assembly of thermally reconfigurable colloidal states, which may be an exceptionally promising way of designing artificial mesostructured composite materials with unique macroscopic properties.[6,38] For example, thermally reconfigurable assembly of anisotropic plasmonic colloids with near-infrared plasmonic properties can enable temperature-dependent solar gain control functionality.[30] Moreover, the application of electric, magnetic, and optical fields could allow for further facile control over the organization of the particles and molecules within the composite, leading to diverse functional properties. Furthermore, with the possibility of utilizing advanced mesoscale colloidal systems[45] having diverse functional properties will boost up future research in the field of LC colloidal composites, which has been largely limited to either low particle concentrations or nanoscale particles, such as dyes, quantum dots, and other nanoscale particles.[46] The ability to achieve dense dispersion of anisotropic micron-sized colloids in nematic LC host opens up the need of further studies on colloids of diverse shapes including bent-core rods,[47] helices,[48] Janus rods,[49] or patchy particles[50–52] with porous nature.

To conclude, we have developed a mesostructured soft matter system that shows uninhibited 3D orientational fluid order of micrometer-sized colloidal and nanometer-sized molecular building blocks, with several low-symmetry phases. Despite having dimensions in the range of hundreds of nanometers to micrometers, larger than surface anchoring extrapolation length, these colloidal rods exhibit interactions with the surrounding LC medium resembling that of nanoparticles. The emergent behavior of these particles partly mimics that of 10-nm-thick colloidal disks,[5] arising from a thermal self-reconfiguration process that controls relative orientations of the molecular and colloidal subsystems. This self-reconfiguration is facilitated by the interplay between anisotropic elastic, steric, and electrostatic colloidal interactions taking place while the anisotropic molecular fluid host maintains a uniform far-field background, regardless of the phase symmetry. The anisotropic microrods are effectively prevented from aggregating due to the combination of surface porosity and slippery molecular coating layers, which also enable self-reconfigurability of the boundary conditions at their surfaces. Phase diagrams of the molecular-colloidal self-assemblies reveal thermally reconfigurable reorientations of both individual colloidal particles and self-assembled nematic and other soft matter states and pre-transitional effects, as well as discuss potential technological utility in terms of realizing pre-designed mesostructured materials. Numerical modeling based on free energy minimization provides helpful insights into the role of pores in modifying surface interactions. On the other hand, our analytical investigation of nematic ordering and phase transformations offers insight into observed spontaneous symmetry breaking and the stabilization of nematic phases with nonstandard symmetries, revealing that by selecting different LC hosts and colloidal particles with varying shapes, and by adjusting the surface textures of these particles, it may be possible to explore and control the formation of diverse mesophases. For example, given our findings described here, it may be possible to obtain a long-range-ordered monoclinic nematic phase from rod-like-only molecular and colloidal building blocks of the hybrid LCs, differing from the rod-disk molecular-colloidal system that we introduced earlier.[5] From an applied perspective, our findings may lead to the design of mesostructured molecular-colloidal composites with pre-engineered physical properties.

METHODS

Synthesis of the porous silica microrods

The synthesis of silica microrods was conducted using an emulsion-templated wet-chemical method. In a typical procedure, 1 g of polyvinylpyrrolidone (PVP) with a molecular weight of 40,000 (Sigma-Aldrich) was added to a 20-mL glass vial and dissolved in 10 mL of 1-pentanol (≥99%, Sigma-Aldrich) through sonication. Once the PVP was completely dissolved, the following components were sequentially added: 950 μL of absolute ethanol (Decon Labs), 280 μL of ultrapure de-ionized water (Millipore system), 100 μL of a 0.18 M aqueous solution of sodium citrate dihydrate (99%, Sigma-Aldrich), and 130 μL of ammonia (28%, Sigma-Aldrich). After each addition, the vial was vigorously shaken using a vortex mixer and then allowed to stand for a few minutes to release any trapped air bubbles. The resulting solution appeared turbid, indicating the formation of an emulsion. Subsequently, 100 μL of tetraethyl orthosilicate (TEOS, 98%, Sigma-Aldrich) was added dropwise, and the solution was gently shaken once again. The vial was then stored at 25°C, and the reaction was allowed to proceed for the next 8 h.

Purification of the microrods

After the completion of the designated reaction time, the solution transformed into a milky white appearance. To separate the as-synthesized rods, the solution underwent centrifugation using a microcentrifuge at a speed of 6,000 rpm for a duration of 10 min. The resulting precipitated rods were subjected to two washes with water, followed by an additional two rounds of washing with ethanol. Each ethanol wash was carried out at 3,000 rpm for 5 min. Last, to enhance monodispersity and eliminate any remaining lightweight impurities, the rods underwent three consecutive centrifugation cycles at a speed of 500 rpm for a duration of 30 min.

Surface functionalization of the microrods

In the subsequent step, the microrods underwent functionalization with a perfluorocarbon surface coating utilizing a two-step method. This method involved a liquid-phase deposition of perfluorocarbon molecules followed by integration with a perfluorocarbon liquid. Initially, 100 μL of 1H,1H,2H,2H-perfluorooctyltriethoxysilane (97%, TCI America) was added to a dispersion of etched silica rods in 900 μL ethanol (200 Proof, DeconLabs). These silica rods were previously dried in an oven at 80°C for 4 h. The resulting mixture was kept at room temperature for 3 h, with occasional shaking. During this process, the perfluorosilane molecules chemically bonded to the surface of the rods, forming a coating. Subsequently, the rods were washed three times with ethanol at 5,000 rpm for 2 min. The sedimented rods were vacuum-dried inside a desiccator and then subjected to heating at 60°C for 1 h. Next, the microrods were immersed in a perfluorocarbon liquid (Fluorinert FC-70, Alfa Aesar) and left

Please cite this article in press as: Ghosh et al., Reconfigurable self-assembly of porous anisotropic colloids in nematic liquid crystals, Matter (2025), https://doi.org/10.1016/j.matt.2025.102563

overnight in a glass desiccator. This immersion facilitated the fusion of the perfluorocarbon oil onto the perfluorosilane-functionalized rods, resulting in a fully covered and stable slippery surface layer. Following the coating process, the perfluorocarbon-coated rods were washed multiple times with ethanol and subsequently redispersed in fresh ethanol before being stored in a vial for future use.

Preparation of LC cells

In a typical experiment, a nanoparticle dispersion of 30 μL was combined with 10 μL of pure 4-cyano-4′-pentylbiphenyl (5CB) obtained from Chengzhi Yonghua Display Materials Co. Ltd. The mixing took place at room temperature. The resulting mixture was then placed inside an oven at 60°C for 2 h to allow complete evaporation of ethanol. Afterward, the isotropic-phase mixture was sonicated in a water bath at 80°C for 2 min, followed by rapid cooling to induce the nematic phase while maintaining continuous mechanical agitation. To separate any aggregates formed during the transition from isotropic to nematic phase (which can sometimes be prompted by the interfacial tension between nematic and isotropic domains), the mixture underwent centrifugation at 1,200 rpm for 3 min, yielding a uniform colloidal dispersion. Although isotropic-to-nematic quenching of colloidal dispersions can generally also yield different samples with gel-like states, including various aggregates, the quenching and material treatment procedures described here are optimized to result in stable colloidal dispersions of nonaggregating particles at high densities.

Next, a diluted dispersion of silica microrods in the LC was infiltrated into a glass cell with a predetermined thickness using capillary forces. To prepare the LC cells with planar surface anchoring, the glass surfaces were spin-coated with a 1 wt % aqueous solution of polyvinyl alcohol (PVA) obtained from Sigma-Aldrich. The coated glass substrates were then baked at 100°C for 1 h. Unidirectional rubbing of the PVA-coated surfaces of the substrates was performed using a soft velvet cloth to define the direction of the boundary conditions for the molecular director, $\mathbf{n}_m$. Subsequently, the glass surfaces were bonded together using UV-curable NOA-65 glue from Norland Products, Inc., which contained spacers such as 40-μm silica spheres to define the desired cell gap upon curing the glue.

Modeling effective anchoring properties of a porous surface

To get insights into how the porous nature of particles alters the LC-surface interactions as compared to what they would be for flat surfaces, we performed modeling of the effective surface anchoring with an idea of coarse-graining the description of these interactions. We first numerically simulate the equilibrium director field $\mathbf{n}_m(\mathbf{r})$ in a box with one boundary being a porous surface described as containing an array of holes of different density (Figure 2A), which was implemented by minimizing the total LC free energy, consisting of bulk energy and surface anchoring contributions:

$$F_{LC} = \int f_{bulk}\, dr^3 + \int f_{surf}\, dr^2 \qquad \text{(Equation 4)}$$

where f_{surf} is the surface energy density given by Equation 1 and f_{bulk} is its bulk counterpart. For simplicity, we adopt the one-constant Frank-Oseen elastic free energy functional:

$$f_{bulk} = \frac{K}{2}|\nabla \mathbf{n}_m|^2 \qquad \text{(Equation 5)}$$

where the average Frank elastic constant is assumed to be $K = 3$ pN. Using our home-built MATLAB program,[33] we carried out the energy-minimization calculation on a regular 3D grid set with 3-nm spacing and with periodic boundary conditions for directions perpendicular to the surfaces, along the z axis (Figure 2A). The porous surface at $z = d$ is numerically represented by square-periodic arrays of topographic features, each with dimensions 9 nm × 9 nm × 45 nm, with the hole area fraction tunable by changing the spacing between the holes. Accordingly, the total energy is integrated carefully over such nonsmooth surface and within the volume adjacent to it. A flat boundary with fixed boundary conditions is placed on the opposite side at $z = 0$ of the volume. The simulation box is typically set to be 150 nm × 150 nm × 150 nm. The (local) surface anchoring coefficient $W_0 = 5.8 \times 10^{-4}$ Jm^{-2} and homeotropic condition for the easy axis $\Theta_e = 0^\circ$ are assumed if not otherwise specified.

After obtaining an equilibrium molecular nematic director field $\mathbf{n}_m(\mathbf{r})$ for such a system with one porous surface, we can then imagine replacing the porous boundary using a flat one, but with different effective surface anchoring coefficients, such that the director alignments and energetic costs roughly remain the same under the ensuing equilibrium states. Considering our geometry (Figure 2A), the overall molecular LC's free energy for such boundary conditions with only flat surfaces is now translationally invariant (in x and y directions parallel to the confining surface) and can be expressed using the following form:

$$F_{LC} \propto W_{eff}\left(\cos^2(\Theta_s) - \cos^2(\Theta_{eff})\right)^2 + K\int_0^d \left(\frac{d\Theta}{dz}\right)^2 dz \qquad \text{(Equation 6)}$$

where Θ is the angle describing director orientation relative to the surface normal and Θ_s is its value at surfaces. Here, the energy-minimizing configuration $\mathbf{n}_m(\mathbf{r})$ can be calculated analytically and the Euler-Lagrange equations for Equation 6 give a linear dependence of $\Theta(z)$ on z (Figure 2B). The linear fits of the computer-simulated $\mathbf{n}_m(\mathbf{z})$ described by $\Theta(z) \cong \langle\Theta(\mathbf{r})\rangle_{x,y}$ were performed, and the resulting slopes and effective boundary values of $\Theta(z)$ were subsequently used to calculate the anchoring coefficients for the substitute flat surface, W_{eff} and Θ_{eff}, whose values are interpreted as "effective" surface anchoring and easy axis angle characteristics of the porous surface. We then performed five independent simulations of $\Theta(\mathbf{r})$ on a large scale around the microrod's surfaces using different director angles on the "frozen" surface $\Theta(z = 0)$ for each set of W_{eff} and Θ_{eff}. To visualize the local perturbation in the molecular alignment induced by the porous microrod with an effective surface anchoring, we performed coarse-grained numerical simulation for coefficients $W_{eff} = 10^{-5}$ Jm^{-2}, and various Θ_{eff} are adopted. The methodology of these simulations is detailed in Mundoor et al.[5] The equilibrium angle θ_c between the background $\mathbf{n}_m$ away from the microrod and the microrod's long axis is estimated by the minimization

of total surface energy integrated over the entire microrod surface (Equation 1). Ignoring the insignificant contribution from the ends of a thin rod, we obtain

$$\sin^2(\theta_c) = \frac{4}{3}\cos^2(\Theta_{eff}) \quad \text{,(Equation 7)}$$

which was computed numerically to determine the values of Θ_{eff} for simulations shown in Figure 3B.

RESOURCE AVAILABILITY

Lead contact

Requests for further information and resources should be directed to and will be fulfilled by the lead contact, Ivan I. Smalyukh (ivan.smalyukh@colorado.edu).

Materials availability

All structural data and information generated in this study are available from the lead contact.

Data and code availability

The data that support the findings of this study are available from the corresponding author upon reasonable request.

ACKNOWLEDGMENTS

We thank P. de Melo, B. Senyuk, and J.-S. Tai for discussions and technical assistance. This research was supported by the US Department of Energy, Office of Basic Energy Sciences, Division of Materials Sciences and Engineering, under contract DE-SC0019293 with the University of Colorado at Boulder. I.I.S. and L.L. acknowledge the hospitality of the International Institute for Sustainability with Knotted Chiral Meta Matter (WPI-SKCM^2) at Hiroshima University during their visits, where they were partly working on this article, and where, in particular, the analytical modeling component of this work was initialized. L.L. also acknowledges the support from the National Science Centre in Poland under the grant no. 2021/43/B/ST3/03135.

AUTHOR CONTRIBUTIONS

I.I.S. conceived and directed this project and supervised experimental and computational research. S.G. developed and planned the experimental methodology and performed synthesis and experimental studies. J-S.W. formulated the theoretical model of surface anchoring due to porous surfaces and performed computer simulation. L.L. developed the Landau-de Gennes theory describing phase transitions and order parameters in the studied system. S.G. and N.G. analyzed the data. S.G., J-S.W., and I.I.S. wrote the manuscript with input from all authors.

DECLARATION OF INTERESTS

The authors declare no conflict of interest.

SUPPLEMENTAL INFORMATION

Supplemental information can be found online at https://doi.org/10.1016/j.matt.2025.102563.

Received: April 26, 2025
Revised: August 26, 2025
Accepted: November 6, 2025

REFERENCES

1. Manoharan, V.N. (2015). Colloidal matter: Packing, geometry, and entropy. Science *349*, 1253751.
2. Anderson, V.J., and Lekkerkerker, H.N.W. (2002). Insights into phase transition kinetics from colloid science. Nature *416*, 811–815.
3. Senyuk, B., Behabtu, N., Martinez, A., Lee, T., Tsentalovich, D.E., Ceriotti, G., Tour, J.M., Pasquali, M., and Smalyukh, I.I. (2015). Three-dimensional patterning of solid microstructures through laser reduction of colloidal graphene oxide in liquid-crystalline dispersions. Nat. Commun. *6*, 7157.
4. Smalyukh, I.I. (2018). Liquid crystal colloids. Annu. Rev. Condens. Matter Phys. *9*, 207–226.
5. Mundoor, H., Wu, J.-S., Wensink, H.H., and Smalyukh, I.I. (2021). Thermally reconfigurable monoclinic nematic colloidal fluids. Nature *590*, 268–274.
6. Mundoor, H., Park, S., Senyuk, B., Wensink, H.H., and Smalyukh, I.I. (2018). Hybrid molecular-colloidal liquid crystals. Science *360*, 768–771.
7. Liu, Q., Ackerman, P.J., Lubensky, T.C., and Smalyukh, I.I. (2016). Biaxial ferromagnetic liquid crystal colloids. Proc. Natl. Acad. Sci. USA *113*, 10479–10484.
8. Poulin, P., Stark, H., Lubensky, T.C., and Weitz, D.A. (1997). Novel colloidal interactions in anisotropic fluids. Science *275*, 1770–1773.
9. Gu, Y., and Abbott, N.L. (2000). Observation of Saturn-ring defects around solid microspheres in nematic liquid crystals. Phys. Rev. Lett. *85*, 4719–4722.
10. Stark, H. (2001). Physics of colloidal dispersions in nematic liquid crystals. Phys. Rep. *351*, 387–474.
11. Lubensky, T.C., Pettey, D., Currier, N., and Stark, H. (1998). Topological defects and interactions in nematic emulsions. Phys. Rev. E *57*, 610–625.
12. Senyuk, B., Liu, Q., He, S., Kamien, R.D., Kusner, R.B., Lubensky, T.C., and Smalyukh, I.I. (2013). Topological colloids. Nature *493*, 200–205.
13. Liu, Q., Senyuk, B., Tasinkevych, M., and Smalyukh, I.I. (2013). Nematic liquid crystal boojums with handles on colloidal handlebodies. Proc. Natl. Acad. Sci. USA *110*, 9231–9236.
14. Martinez, A., Ravnik, M., Lucero, B., Visvanathan, R., Žumer, S., and Smalyukh, I.I. (2014). Mutually tangled colloidal knots and induced defect loops in nematic fields. Nat. Mater. *13*, 258–263.
15. Sacanna, S., Irvine, W.T.M., Chaikin, P.M., and Pine, D.J. (2010). Lock and key colloids. Nature *464*, 575–578.
16. Chaikin, P.M., Lubensky, T.C., and Witten, T.A. (1995). Principles of Condensed Matter Physics (Cambridge university press Cambridge).
17. De Gennes, P.-G., and Prost, J. (1993). The Physics of Liquid Crystals (Oxford university press).
18. Ravnik, M., Čopar, S., and Žumer, S. (2015). Particles with changeable topology in nematic colloids. J. Phys. Condens. Matter *27*, 354111.
19. Ravnik, M., Alexander, G.P., Yeomans, J.M., and Žumer, S. (2011). Three-dimensional colloidal crystals in liquid crystalline blue phases. Proc. Natl. Acad. Sci. USA *108*, 5188–5192.
20. Kuijk, A., Van Blaaderen, A., and Imhof, A. (2011). Synthesis of monodisperse, rodlike silica colloids with tunable aspect ratio. J. Am. Chem. Soc. *133*, 2346–2349.
21. Hagemans, F., van der Wee, E.B., van Blaaderen, A., and Imhof, A. (2016). Synthesis of Cone-Shaped Colloids from Rod-Like Silica Colloids with a Gradient in the Etching Rate. Langmuir *32*, 3970–3976. https://doi.org/10.1021/acs.langmuir.6b00678.
22. Smalyukh, I.I. (2018). Liquid Crystal Colloids. Annu. Rev. Condens. Matter Phys. *9*, 207–226. https://doi.org/10.1146/annurev-conmatphys-033117-054102.
23. Senyuk, B., Glugla, D., and Smalyukh, I.I. (2013). Rotational and translational diffusion of anisotropic gold nanoparticles in liquid crystals controlled by varying surface anchoring. Phys. Rev. E *88*, 062507.
24. Loudet, J.C., Hanusse, P., and Poulin, P. (2004). Stokes drag on a sphere in a nematic liquid crystal. Science *306*, 1525.
25. Pujala, R.K., and Dhara, S. (2019). Colloidal analogues of polymer chains, ribbons and 2D crystals employing orientations and interactions of nanorods dispersed in a nematic liquid crystal. Sci. Rep. *9*, 4652.

26. Wong, T.-S., Kang, S.H., Tang, S.K.Y., Smythe, E.J., Hatton, B.D., Grinthal, A., and Aizenberg, J. (2011). Bioinspired self-repairing slippery surfaces with pressure-stable omniphobicity. Nature *477*, 443–447.

27. Wu, Z., Troll, J., Jeong, H.-H., Wei, Q., Stang, M., Ziemssen, F., Wang, Z., Dong, M., Schnichels, S., Qiu, T., and Fischer, P. (2018). A swarm of slippery micropropellers penetrates the vitreous body of the eye. Sci. Adv. *4*, eaat4388.

28. Wang, X., Zhou, Y., Palacio-Betancur, V., Kim, Y.K., Delalande, L., Tsuei, M., Yang, Y., De Pablo, J.J., and Abbott, N.L. (2019). Reconfigurable Multicompartment Emulsion Drops Formed by Nematic Liquid Crystals and Immiscible Perfluorocarbon Oils. Langmuir *35*, 16312–16323. https://doi.org/10.1021/ACS.LANGMUIR.9B02864/SUPPL_FILE/LA9B02864_SI_001.PDF.

29. Liu, Q., Yuan, Y., and Smalyukh, I.I. (2014). Electrically and optically tunable plasmonic guest-host liquid crystals with long-range ordered nanoparticles. Nano Lett. *14*, 4071–4077. https://doi.org/10.1021/nl501581y.

30. Ghosh, S., and Smalyukh, I. (2022). Electrical Switching of Nematic Plasmonic Nanocolloids for Infrared Solar Gain Control. Adv. Opt. Mater. *10*, 2201513. https://doi.org/10.1002/ADOM.202201513.

31. Mundoor, H., Senyuk, B., and Smalyukh, I.I. (2016). Triclinic nematic colloidal crystals from competing elastic and electrostatic interactions. Science *352*, 69–73.

32. Mundoor, H., Senyuk, B., Almansouri, M., Park, S., Fleury, B., and Smalyukh, I.I. (2019). Electrostatically controlled surface boundary conditions in nematic liquid crystals and colloids. Sci. Adv. *5*, eaax4257.

33. Zhou, Y., Senyuk, B., Zhang, R., Smalyukh, I.I., and de Pablo, J.J. (2019). Degenerate conic anchoring and colloidal elastic dipole-hexadecapole transformations. Nat. Commun. *10*, 1000. https://doi.org/10.1038/s41467-019-08645-9.

34. Jerome, B. (1991). Surface effects and anchoring in liquid crystals. Rep. Prog. Phys. *54*, 391–451.

35. Turiv, T., Lazo, I., Brodin, A., Lev, B.I., Reiffenrath, V., Nazarenko, V.G., and Lavrentovich, O.D. (2013). Effect of collective molecular reorientations on Brownian motion of colloids in nematic liquid crystal. Science *342*, 1351–1354.

36. Lapointe, C.P., Mason, T.G., and Smalyukh, I.I. (2009). Shape-controlled colloidal interactions in nematic liquid crystals. Science *326*, 1083–1086.

37. Yoshizawa, A., Nishizawa, A., Takeuchi, K., Takanishi, Y., and Yamamoto, J. (2010). Interlayer Interactions Induced by Amphiphilicities of a Rod-Like Molecule Produce Frustrated Structures in Conventional Calamitic Phases. J. Phys. Chem. B *114*, 13304–13311. https://doi.org/10.1021/jp106269m.

38. Ravnik, M., and Žumer, S. (2009). Landau–de Gennes modelling of nematic liquid crystal colloids. Liq. Cryst. *36*, 1201–1214.

39. Senyuk, B., Adufu, R.E., and Smalyukh, I.I. (2022). Electrically powered locomotion of dual-nature colloid-hedgehog and colloid-umbilic topological and elastic dipoles in liquid crystals. Langmuir *38*, 689–697.

40. Selinger, J.V. (2016). Introduction to the Theory of Soft Matter (Springer). https://doi.org/10.1007/978-3-319-21054-4.

41. Gramsberger, E.P., Longa, L., and de Jeu, W.H. (1986). Landau Theory of the Nematic - Isotropic Phase Transition. Phys. Report *135*, 195–257.

42. Allender, D., and Longa, L. (2008).). Landau-de Gennes Theory of Biaxial Nematics Re-examined. Phys. Rev. E *78*, 011704.

43. Spencer, A.J.M., and Rivlin, R.S. (1958). The theory of matrix polynomials and its application to the mechanics of isotropic continua. Arch. Ration. Mech. Anal. *2*, 309–336.

44. Spencer, A.J.M., and Rivlin, R.S. (1958). Finite integrity bases for five or fewer symmetric 3× 3 matrices. Arch. Ration. Mech. Anal. *2*, 435–446.

45. Kowerdziej, R., Ferraro, A., Zografopoulos, D.C., and Caputo, R. (2022). Soft-Matter-Based Hybrid and Active Metamaterials. Adv. Opt. Mater. *10*, 2200750.

46. Boles, M.A., Engel, M., and Talapin, D.V. (2016). Self-assembly of colloidal nanocrystals: From intricate structures to functional materials. Chem. Rev. *116*, 11220–11289.

47. Bisoyi, H.K., and Kumar, S. (2011). Liquid-crystal nanoscience: an emerging avenue of soft self-assembly. Chem. Soc. Rev. *40*, 306–319.

48. Yang, Y., Chen, G., Martinez-Miranda, L.J., Yu, H., Liu, K., and Nie, Z. (2016). Synthesis and liquid-crystal behavior of bent colloidal silica rods. J. Am. Chem. Soc. *138*, 68–71.

49. Ghosh, S., and Ghosh, A. (2018). Mobile nanotweezers for active colloidal manipulation. Sci. Robot. *3*, eaaq0076. https://doi.org/10.1126/scirobotics.aaq0076.

50. Ghosh, S., and Ghosh, A. (2019). All optical dynamic nanomanipulation with active colloidal tweezers. Nat. Commun. *10*, 4191. https://doi.org/10.1038/s41467-019-12217-2.

51. He, M., Gales, J.P., Ducrot, É., Gong, Z., Yi, G.-R., Sacanna, S., and Pine, D.J. (2020). Colloidal diamond. Nature *585*, 524–529.

52. Sacanna, S., and Pine, D.J. (2011). Shape-anisotropic colloids: Building blocks for complex assemblies. Curr. Opin. Colloid Interface Sci. *16*, 96–105.